Korean J. Chem. Eng., 34(11), 2861-2869 (2017)
DOI: 10.1007/s11814-017-0177-z

pISSN: 0256-1115
eISSN: 1975-7220

Experimental and theoretical analysis of element mercury adsorption on Fe_3O_4/Ag composites

Lu Dong*, Jiangkun Xie, Guangping Fan**, Yaji Huang*,†, Jun Zhou**, Qingke Sun*, LiangWang*, Zhengwen Guan**, Di Jiang**, and Ye Wang****

*Key Laboratory of Energy Thermal Conversion and Control of Ministry of Education, School of Energy and Environment, Southeast University, Nanjing 210096, China
**China Construction Power and Environment Engineering Co., Ltd., Nanjing 210008, China
(*Received 15 July 2016 • accepted 2 July 2017*)

Abstract−A novel magnetic nano-sorbent Fe_3O_4/Ag was synthesized and applied to capture the elemental mercury from the simulated flue gas. The morphology, components and crystal phase of the sorbents were characterized by transmission electron microscope (TEM), energy dispersive spectrometry (EDS) and X-ray diffraction (XRD), respectively. The mercury removal performance of the sorbents was investigated through the fixed-bed tests. The results indicated that silver was successfully loaded on the surface of Fe_3O_4 particles, which could significantly enhance the Hg^0 removal performance of the sorbents. Flue gas components, including CO_2, SO_2, and NO, have little impact on the Hg^0 removal performance of Fe_3O_4/Ag sorbents, while O_2 has a slightly positive effect. The Hg^0 removal efficiency decreased with the increasing of temperature, Hg^0 inlet concentration and gas hourly space velocity. Only one broad mercury desorption peak at approximately 210 °C could be observed during the temperature-programmed desorption (TPD) process, which indicated that mercury species existing on the surface of Fe_3O_4/Ag sorbents might be elemental mercury instead of oxidized mercury. Furthermore, the reusability tests showed that the Fe_3O_4/Ag sorbents could be efficiently regenerated and reused. Finally, the theoretical analysis based on the DFT method showed that a weak chemisorption of Hg^0 on Fe_3O_4 sorbents changed to a strong chemisorption when silver was loaded. The results of theoretical analysis conformed to the experiments results well.

Keywords: Hg^0, Sorbent, Magnetic, $Dmol^3$

INTRODUCTION

Mercury, as one of the heavy metals emitted from industry, has attracted increasing concern due to its high volatility, toxicity, easy bioaccumulation in the environment, and severe health effects [1]. It is believed that, in anthropogenic activities, coal combustion is a major source of mercury emissions. Therefore, it is critical to minimize mercury emissions from existing industrial mercury emitters such as coal-fired power plants [2].

The mercury speciation in coal-fired flue gas can be classified into three forms: elemental (Hg^0), oxidized (Hg^{2+}), and particulate bound (Hg^P) mercury, which are mainly dependent on the combustion conditions and the chlorine content in the coal [3]. Hg^{2+} can be effectively trapped by the wet flue gas desulfurization equipment (WFGD) due to its easy solubility. Hg^P can be removed by particulate control devices (PCDs) [4]. In contrast, the removal of Hg^0 is much harder due to its high volatility and extremely low solubility [5]. Thus, it is necessary to develop effective technologies to remove Hg^0. Activated carbon injection (ACI) into the flue gas to absorb Hg^0 directly and subsequently removed by existing PCDs appears to be an efficient and cost-effective process to capture mercury in power plant stacks [6,7]. An obvious shortcoming of ACI technology is the limited use times of the sorbents, resulting in high operating costs [8]. Whereas, noble metals, including palladium (Pd), platinum (Pt), gold (Au) and silver (Ag), based sorbents capture mercury via amalgamation that can be regenerated in elevated temperature for unlimited times and maintain good performance [9]. Silver-based sorbents, such as carbon nanotube [10] and graphene [11], have been experimentally investigated to remove Hg^0 due to its much lower cost compared to other metals. However, it is impossible to separate these kinds of sorbents from fly ashes when both of them have been captured by the PCDs [12]. Interestingly, magnetically separable sorbents have been proposed in recent years. Several novel magnetic sorbents, including FeSi-Ag and MagZ-Ag, have been developed to remove mercury from flue gas, which are easy to separate from fly ashes by magnetic separation [13].

Although mercury adsorption on silver based sorbents has been investigated experimentally, the detailed mechanism of this reaction is still unclear. Fortunately, quantum chemistry methods based on density functional theory (DFT) have been increasingly used to investigate the interaction of mercury with Cu, Ni, Pd, Ag, and Au surfaces [10] at the molecular-electronic level. The DFT calculation of TiO_2-based Ag sorbent predicted that the reactivity of the Ag_n/TiO_2 composites was higher than both the bare Ag_n cluster and the TiO_2(110) surface due to the synergetic effect of Ag_n and

†To whom correspondence should be addressed.
E-mail: heyyj@seu.edu.cn
‡This paper is reported in the 11th China-Korea Clean Energy Workshop.
Copyright by The Korean Institute of Chemical Engineers.

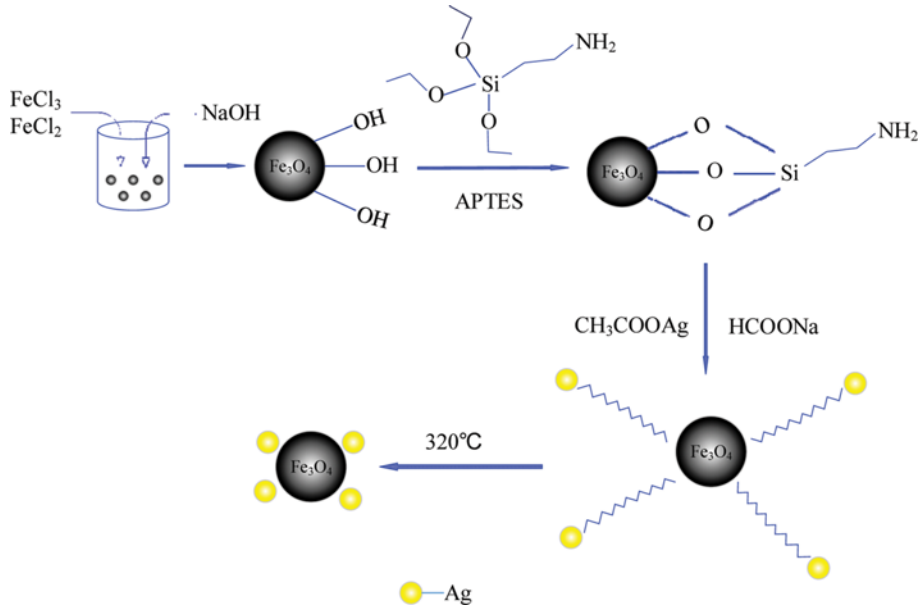

Fig. 1. Schematic illustration of the preparation of Fe_3O_4/Ag composites.

TiO_2 [14].

To the best of our knowledge, the theoretical study of Hg^0 adsorption over Fe_3O_4 or Fe_3O_4/Ag sorbents has never been reported in the literature. In the present work, we performed a comparative study of adopting Fe_3O_4(111) surface and Ag adsorbed Fe_3O_4(111) surface as the adsorptive surface for Hg^0 adsorption by DFT calculations. Our goal was to achieve a better understanding of the interaction between Hg^0 and sorbents through adsorption geometry and adsorption energy, which could also provide an insightful explanation of our experiments.

In this study, the mercury sorbents synthesized by incorporating silver on Fe_3O_4 nanoparticles are presented. The characterization of the sorbents was researched by XRD, TEM and EDS. The Hg^0 removal performance of the sorbents was investigated in a fixed-bed reactor. The effects of temperature, flue gas components, Hg^0 inlet concentration, gas hourly space velocity were all considered. The TPD analysis and reusability tests of the sorbents were also investigated. A theoretical analysis based on DFT calculations was performed to obtain the adsorption energy of Hg^0 on Fe_3O_4(111) surface and Ag/Fe_3O_4(111) surface.

EXPERIMENT AND COMPUTATIONAL METHOD

1. Experimental Section

1-1. Sorbents Preparation

Analytical grades of ferric chloride hexahydrate ($FeCl_3 \cdot 6H_2O$), ferrous chloride tetrahydrate ($FeCl_2 \cdot 4H_2O$), hydrochloric acid (HCl), sodium hydroxide (NaOH), (3-aminopropyl) triethoxysilane (APTES), silver acetate (CH_3COOAg), sodium format (HCOONa), and absolute ethanol (C_2H_6O) were used as received.

The Fe_3O_4 nanoparticles were prepared through conventional chemical co-precipitation of Fe(II) and Fe(III) chlorides (Fe^{II}/Fe^{III} ratio=0.5) with 1.5 M NaOH reported previously [15]. The black precipitate was separated by magnetic force, followed by washing several times with ethanol, and dispersed in ethanol to form 5 g/*l* solution. The modification of Fe_3O_4 nanoparticles with APTES was prepared through the method reported in the previous literature [16]. The Fe_3O_4/APTES was dispersed in ethanol to form 1 g/L solution and added 0.1 M CH_3COOAg dropwise while stirring at 40 °C for 2 h, followed by adding 0.1 M HCOONa for the reduction of Ag^+ to Ag^0. Subsequently, theFe_3O_4/Ag particles were magnetically separated, washed several times with ethanol and then dried at 320 °C for 4 h. The loading amount of silver was about 1 wt% of Fe_3O_4. The preparation of Fe_3O_4/Ag composites is illustrated in Fig. 1.

1-2. Characterization

The crystal structure of the Fe_3O_4/Ag sorbents was identified by a powder X-ray diffraction (XRD) obtained with a Japan Rigaku DMax-γA rotation anode X-ray diffract meter equipped with graphite monochromatized Cu K_α radiation. The micrograph structure and the elements on the surface of the sorbents were analyzed by transmission electron microscopy (TEM) analysis and energy dispersive spectroscopy (EDS) by the use of Tecnai G20.

1-3. Experimental Method

The experimental apparatus is descripted schematically in Fig. 2. The device mainly consisted of gas preparation system, detection system and fixed-bed reactor. The simulated flue gas was a mixture of 6% O_2, 8% CO_2, 500 ppm SO_2, 300 ppm NO, and balanced N_2, with a total flow rate of 2,000 mL·min^{-1}. One stream of N_2 with a flow rate of 300 mL·min^{-1} was purged through a mercury permeation device placed in a sealed U-shaped quartz tube to introduce elemental mercury vapor to the system. The Hg^0 inlet concentration (controlled by the temperature of water bath) of the system variable was in the range of 22.8 to 61.5 μg·m^{-3}. The Hg^0 and the simulated flue gas of different species were premixed before passing through the fixed-bed reactor. The adsorption tests were conducted by packing 200 mg sorbents mixed with 300 mg SiO_2 particles into a quartz glass tube reactor (L-100 mm and D-16 mm),

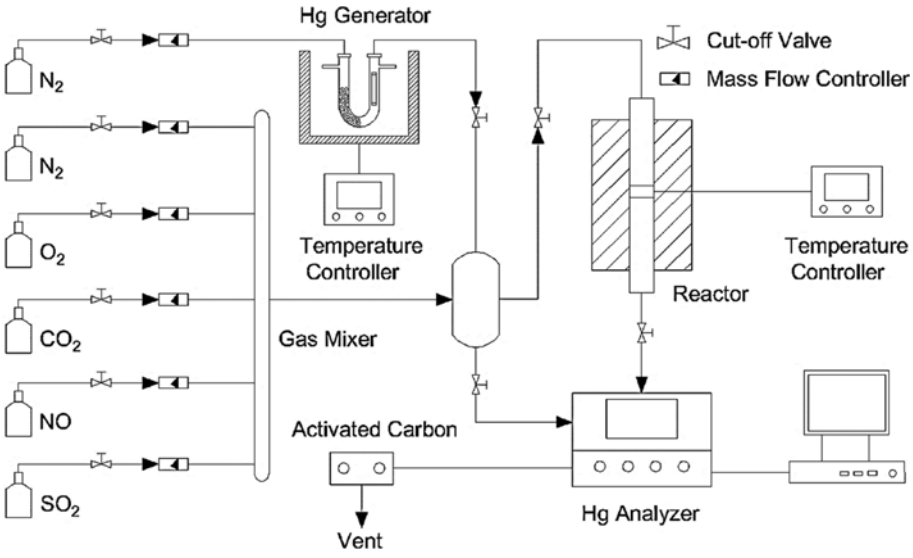

Fig. 2. Schematic diagram of fixed-bed system.

which was located in a temperature-controlled oven. The size of sorbents and SiO_2 particles was meshed in the range of 40 to 60 meshes, and the gas hourly space velocity of the typical condition was set at about $3.12\times10^5\ h^{-1}$. The Hg^0 concentration of the outlet gas was detected by an online VM3000 vapor-mercury analyzer (Mercury Instruments, Germany). Vent gas was purified using activated carbon and sodium hydroxide solution to avoid air pollution. Before each test, the mixed gas was diverted to the bypass line to determine the baseline of Hg^0 concentration.

The Hg^0 removal efficiency η was calculated according to the following equation:

$$\eta=(1-C/C_0) \quad (1)$$

where C_0 is the inlet Hg^0 concentration, and C denotes the outlet Hg^0 concentration at the end of 2 h adsorption ($\mu g\cdot m^{-3}$).

2. Computational Models and Method

The DFT calculation was implemented in the program of the DMol^3 package [17]. The Perdew-Burke-Ernzerhof (PBE) functional within the generalized gradient approximation was used (GGA) method and numerical plus polarization (DNP) basis set were employed to describe exchange and correlation effects of adsorption energy from the fully optimized geometry [18]. DFT semi-core pseudopods (DSPP) [19] were used for Hg atoms, Fe atoms, and Ag atoms, whereby the outer electrons are treated as valence electrons and the inner electrons are replaced by a simple potential including some degree of relativistic effects. All electron method was used for all O atoms.

A Monkhorst-Pack mesh k-points grid of 4×4×1 was used to simplify the Brillouin zone [20]. A spin-unrestricted scheme was used to deal with the electronically open shell system intrinsic to Fe_3O_4 [21]. The calculation convergence criteria for the tolerances of SCF, energy, displacement, and force were 1.0×10^{-6}, 1.0×10^{-5} Ha, 0.002 Ha·Å^{-1}, and 0.005 Å, respectively. To test the computational accuracy, we calculated the lattice constant of bulk Fe_3O_4, getting the optimized value of 8.446 Å, which was in reasonable agreement with the experimental value of 8.396 Å [21].

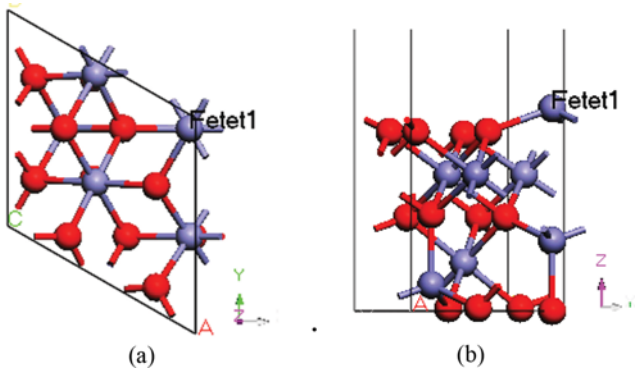

Fig. 3. Schematic top and side views for the Fetet1-terminated surface of Fe_3O_4(111) ((a) Top view, (b) Side view) (red spheres represent the O atoms, and the blue spheres represent the Fe atoms).

Previous research has shown that Fe_3O_4(111) surface is a predominant natural growth face and its catalyst activity is higher than that of other surfaces [22]; the (111) crystal surface has been used to investigate the adsorption of alkali [20], CO_2 [21], H_2 [23], and H_2O [24].

In present work, the Fe_3O_4(111) surface terminated with Fetet1 was chosen as the model to investigate the interaction of Hg^0 and Ag with the Fe_3O_4(111) surface as shown in Fig. 3. We used a model system with eight layers, in which the top two Fe atom layers and two O atom layers were relaxed, and the bottom four layers were fixed during the optimization process [20].

The adsorption energy (E_{ads}) was calculated according to the following equation:

$$\Delta E_{ads}=E_{adsorbate/sorbent}-(E_{adsorbate}+E_{sorbent}) \quad (2)$$

where ΔE_{ads} is the adsorption energy, $E_{adsorbate/sorbent}$ is the total energy of the adsorbed molecule on the Fe_3O_4(111) surface, $E_{adsorbate}$ is the energy of isolated adsorbed molecule (Hg^0 or Ag) in the vacuum, and $E_{sorbent}$ is the energy of the surface. A negative E_{ads} value

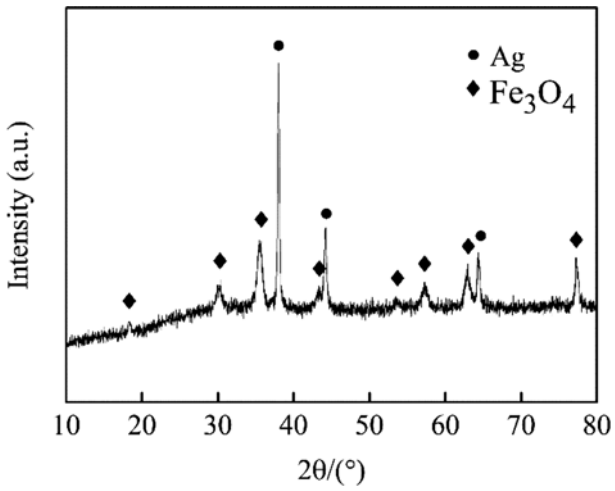

Fig. 4. XRD pattern of the as-synthesized Fe_3O_4/Ag nanocomposites.

corresponds to a stable adsorption system, a more negative value represents stronger adsorption interaction.

RESULTS AND DISCUSSION

1. Sorbents Characterization

The phase of Fe_3O_4/Ag nanoparticle crystal was examined by XRD as shown in Fig. 4. The diffraction peaks at 2θ values of 18.32°, 30.10°, 35.51°, 43.16°, 53.54°, 57.01°, and 62.62° could be ascribed to the crystal surfaces of Fe_3O_4(111), (220), (311), (400), (442), (511) and (440), confirming the existence of the Fe_3O_4 crystal (JCPDS No. 65-3107). The diffraction peaks at 2θ values of 38.10°, 44.32°, and 77.40° could be ascribed to the crystal surface of Ag (111), (200), (220), and (311), indicating the existence of the Ag (JCPDS No. 04-0783) crystal. It can be concluded that the silver coated Fe_3O_4 sorbents were successfully synthesized in our sorbents preparation.

To further explore the morphology of the as-synthesized Fe_3O_4/Ag, a TEM examination was performed and the image is shown in Fig. 5(a). The black region in this image could be ascribed to the crystalline Ag, and the gray region could be regarded as Fe_3O_4 crystal. From the high-resolution (10 nm) TEM image of Fe_3O_4/Ag, the measured interplanar spacing for the lattice fringe of 0.254 nm matched the (111) lattice plane of Ag, while the fringe of 0.487 nm matched the (111) lattice plane of Fe_3O_4. To determine the elemental compositions of the nanocomposites, EDS spectrum in situ composition analysis was performed as shown in Fig. 5(b). The characteristic peaks of Fe, Si, and Ag confirmed that the Fe_3O_4/Ag samples were composed of Fe, Si, and Ag elements, further validating the compositional results of XRD, which indicated that the Fe_3O_4/Ag nanocomposite has been successfully synthesized. The presence of the Cu peak was due to the copper screen used in the sample preparation for TEM analysis.

2. Adsorption Experiments

2-1. Hg^0 Removal Performance

We tested the sorbents in a fixed-bed react system. The Hg^0 removal efficiency of Fe_3O_4 sorbent with and without modified by silver were both tested, and the results are shown in Fig. 6. It was found that the Hg^0 removal efficiency of the raw Fe_3O_4 was lower than 35% indicated a poor Hg^0 adsorption performance. By contrast, Fe_3O_4/Ag showed a great activity of Hg^0 removal with the removal efficiency of more than 91%. It can be concluded that silver could greatly enhance the Hg^0 removal ability of Fe_3O_4 sorbent due to the strong amalgamation with mercury, and Ag-Hg alloy might be formed on the surface of the sorbents [22]. Silver nanoparticles on the surface became the main active sites and dominated the Hg^0 capture. Compared to previous studies, the mercury removal efficiency of Fe_3O_4/Ag sorbents was poorer than MagZ-Ag sorbents [13], which has a larger specific surface might bring more silver loading and beneficial to a higher mercury capture ability.

2-2. Effects of Different Gas Components

Generally, the flue gas from coal-fired power plants contains O_2,

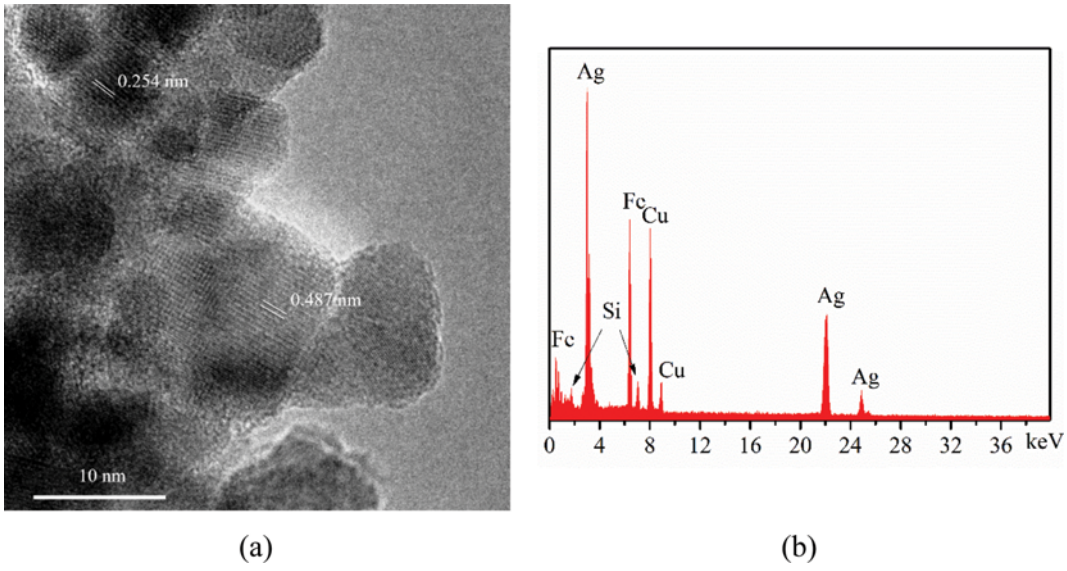

Fig. 5. The TEM image (a) and EDS image (b) of the as-synthesized Fe_3O_4/Ag nanocomposite.

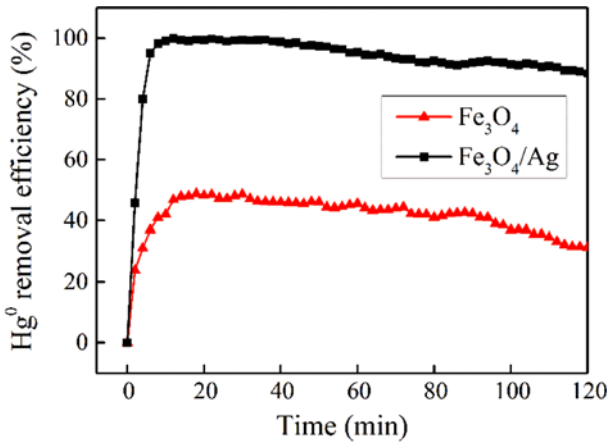

Fig. 6. Hg^0 adsorption performance of as-synthesized sorbents (Conditions: N_2, 38.5 μg/m^3 Hg^0, 100 °C, 3.12×10^5 h^{-1}).

CO_2 and several acid gases including SO_2 and NO in the range from a few hundred to a few thousand parts per million. O_2, CO_2, SO_2, and NO may have an effect on Hg^0 removal performance [13, 26]. Hence, 6% O_2, 8% CO_2, 500 ppm SO_2, and 300 ppm NO were chosen to investigate the impact, and the adsorption temperature was set at 120 °C, which agreed well with the actual flue gas condition before the bag-house filter [7]. The effects of different gas components on the Hg^0 adsorption performance are depicted in Fig. 7. Results showed that the presence of O_2 may have a positive effect on Hg^0 capture of the both sorbents. Previous studies have proved that O_2 efficiently promoted the Hg^0 adsorption on iron oxide nanoparticles [3,26]. The CO_2 showed nearly no effects on Hg^0 removal of these two sorbents. The SO_2 and NO species existing in simulated flue gas also had no obvious effects on Hg^0 capture performance of Fe_3O_4/Ag sorbents, which agreed with previous works that Ag-Hg amalgamation might not be affected by the acid flue gas composition [11,13]. As to bare Fe_3O_4 sorbents, the SO_2

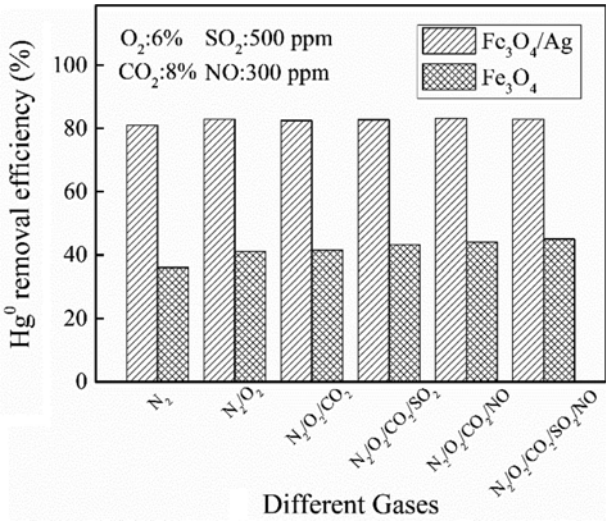

Fig. 7. Effect of different gas composition on the Hg^0 adsorption performance (Conditions: 38.5 μg/m^3 Hg^0, 120 °C , 3.12×10^5 h^{-1}).

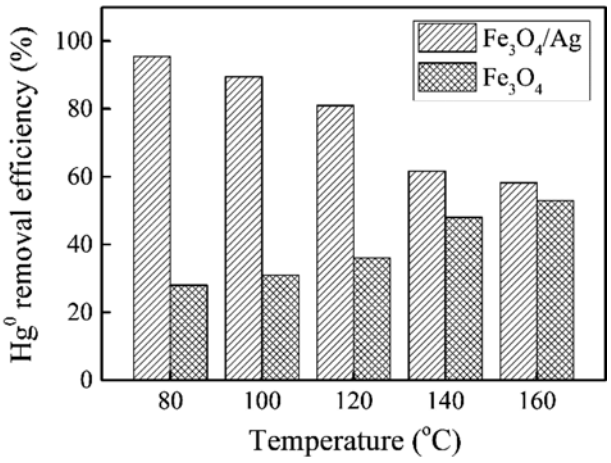

Fig. 8. Effects of temperature on the Hg^0 adsorption performance (Conditions: 6% O_2, 8% CO_2, 500 ppm SO_2, 300 ppm NO, 38.5 μg/m^3 Hg^0, 3.12×10^5 h^{-1}).

and NO both improved Hg^0 capture, which was similar to previous study that the Hg^0 capture ability of iron oxides could be enhanced by acid flue gas components [26]. The difference of the acid flue gas components impact between the two kinds of sorbents could be explained with the reason that the Fe_3O_4 particles coated with silver reduced the contact surface between mercury and Fe_3O_4 particles, which could abate the interaction of acid flue gases with Fe_3O_4. It can be concluded that the Fe_3O_4/Ag sorbents possessed an excellent tolerance of acid gases and have a potential to be applied to remove mercury in the actual flue gas.

2-3. Effects of Temperature

Fig. 8 shows the Hg^0 removal efficiencies over these two kinds of sorbents under various reaction temperatures. The results indicated that increasing adsorption temperature has a negative impact on Hg^0 removal of Fe_3O_4/Ag sorbents while a promotion effect on bare Fe_3O_4 sorbents. When adsorption temperature increased from 80 to 160 °C, Hg^0 removal efficiency of Fe_3O_4/Ag decreased greatly from almost 100% to 57.8%. Especially, when the temperature was above 120 °C, the removal efficiency dropped rapidly and dramatically. The interaction of mercury with Fe_3O_4/Ag sorbents could be divided into the physisorption of mercury on particles and the Hg-Ag amalgamation. However, the interaction would be weakened at an elevated temperature for the reason that the physisorption was exothermic and the amalgamation decomposed to release mercury to the gas phase [28]. The mercury removal ability of Fe_3O_4 sorbents was improved with the increasing of temperature due to the interaction of mercury with metal oxides being mainly attributed to chemisorption, which could be enhanced at an elevated temperature [26]. However, the Hg^0 removal efficiency of Fe_3O_4 sorbents was always less than that of Fe_3O_4/Ag sorbents at the investigated temperatures.

The temperature of flue gas before bag-filter was kept over 120 °C in order to avoid the moisture condensing, which needed the sorbents to have a relative excellent adsorption performance. The Hg^0 removal efficiency of the as-synthesized Fe_3O_4/Ag sorbents at 120 °C was 81.2% as shown in Fig. 8, which might be high enough to remove Hg^0 from the flue gas.

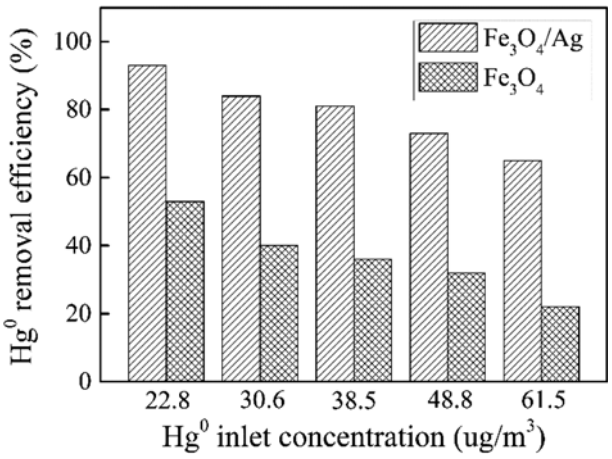

Fig. 9. Effects of Hg^0 inlet concentration on the Hg^0 adsorption performance (Conditions: 6% O_2, 8% CO_2, 500 ppm SO_2, 300 ppm NO, $3.12\times10^5\ h^{-1}$, 120 °C).

2-4. Effects of Hg^0 Inlet Concentration

According to the two-film theory, Hg^0 adsorption ability can be influenced by Hg^0 partial pressure, which is determined by the Hg^0 inlet concentration [29]. The effects of Hg^0 inlet concentration on Hg^0 removal efficiency were studied and the results are shown in Fig. 9. As illustrated in Fig. 9, the two kinds of sorbents showed a similar tendency that the Hg^0 removal efficiency of the sorbents both decreased with the increasing of the Hg^0 inlet concentration. The phenomenon can be explained by the reason that the increasing of Hg^0 inlet concentration resulted in increasing the number of Hg^0 molecules through the reactor per unit time, which could decrease the relative molar ratio of sorbents weight to Hg^0 concentration. The redundant Hg^0 in flue gas could not be captured by a certain amount of sorbents and would remain in the flue gas and be detected by the mercury monitor. Herein, the Hg^0 removal efficiency of the both sorbents maintains a monotonic decrease.

2-5. Effects of Gas Hourly Space Velocity

The Hg^0 removal ability of the Fe_3O_4/Ag and Fe_3O_4 sorbents with various gas hourly space velocities (GHSV) was tested as described in Fig. 10. It was clearly observed that the Hg^0 removal efficiencies were gradually decreased with the increasing of gas hourly space velocity, no matter whether the Fe_3O_4 sorbents were loaded with silver or not. At a lower space velocity of $2.53\times10^5\ h^{-1}$, the Hg^0 removal efficiency of the Fe_3O_4/Ag and Fe_3O_4 sorbent could be achieved 92.5% and 43.5%, respectively, while the Hg^0 removal efficiency dramatically decreased to 51.6% and 22.5%, respectively, when the space velocity elevated to $9.24\times10^5\ h^{-1}$. It might be the reason that an elevated space velocity led to a shorter residence time of the simulated flue gas in the fixed-bed reactor, which meant a shorter contact and adsorption time between the flue gas and the sorbents. As to the actual operation, choosing an appropriate gas hourly space velocity to reach a certain Hg^0 removal efficiency was necessary.

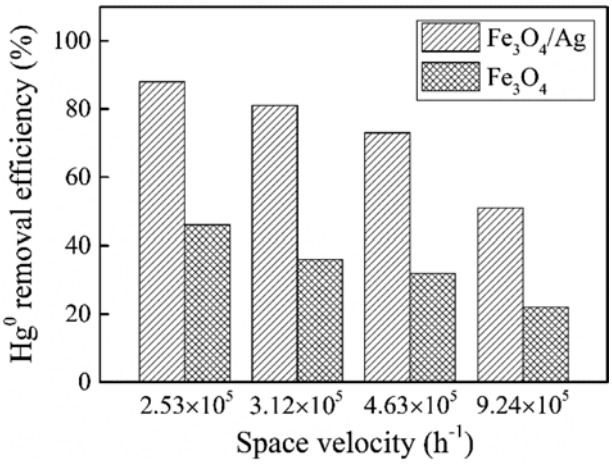

Fig. 10. Effects of space velocity on the Hg^0 adsorption performance (Conditions: 6% O_2, 8% CO_2, 500 ppm SO_2, 300 ppm NO, 38.5 μg/m³ Hg^0, 120 °C).

2-6. Hg-TPD Analysis

To identify the speciation of mercury compounds on the surface of the sorbents after sorption tests, the decomposition characteristics of the mercury species were investigated by temperature-programmed desorption (TPD) method in this study, which was widely used as an efficient technique to distinguish mercury species on solid surface [30-32]. In this study, the TPD experiment of the Fe_3O_4/Ag sorbents was performed following the mercury removal tests in the atmosphere of simulated flue gas including N_2, O_2, CO_2, SO_2 and NO. The Hg-TPD curve was obtained under the heating rate of 4 °C/min and the results are shown in Fig. 11. Only one broad peak at approximately 210 °C can be observed during desorption process, which started from 80 °C to 360 °C (maximum at 210 °C). It can be inferred that mercury on the surface of Fe_3O_4/Ag sorbents began to release at 80 °C, and almost evaporated while the temperature was higher than 360 °C. According to mercury compounds desorption characteristics investigated in previous study, the decomposition of $HgCl_2$, HgO and $HgSO_4$ ranged from 45 °C to 300 °C, 382 °C to 604 °C, 402 °C to 630 °C, respectively [32]. $HgCl_2$ could not be formed on the surface of sorbents due to the absence of chlorine species in our simulated flue gas. The results indicated that mercury desorbed from the surface of sorbents might be the decomposition of the silver-mercury amalgam [11,13,30]. The mercury species existing on the surface of the sorbents might

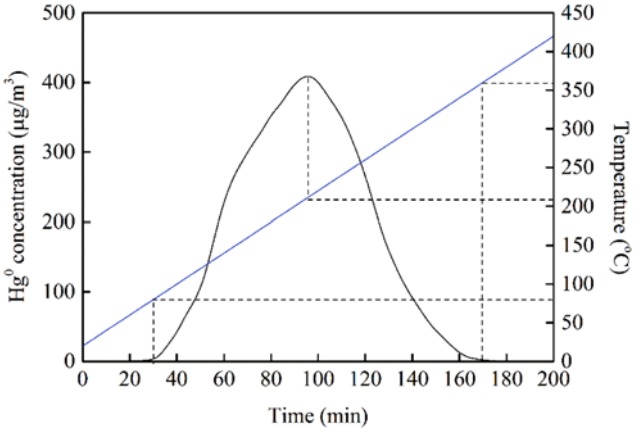

Fig. 11. The Hg^0 desorption curves over tested Fe_3O_4/Ag sorbents.

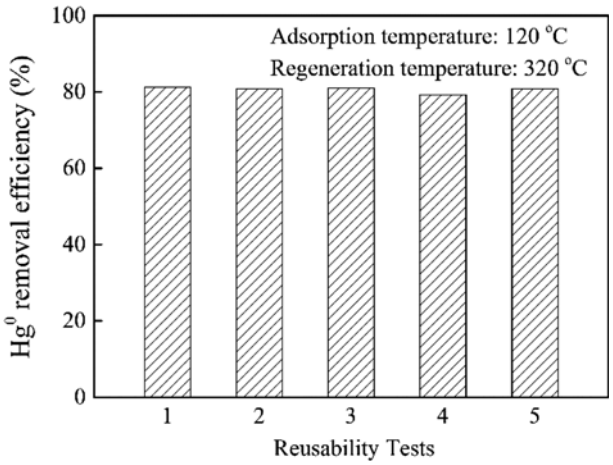

Fig. 12. The reusability test of Fe_3O_4/Ag sorbents for Hg^0 removal efficiency (Conditions: 6% O_2, 8% CO_2, 500 ppm SO_2, 300 ppm NO, 38.5 μg/m^3 Hg^0, 3.12×10^5 h^{-1}, 120 °C).

be elemental mercury instead of oxidized mercury ($HgCl_2$, HgO and $HgSO_4$).

2-7. Reusability Tests of the Sorbents

Reusability is one of the most important characteristics of mercury removal sorbents. Thermal treatment is considered an effective approach for sorbents regeneration. For the as-synthesized Fe_3O_4/Ag sorbents, the adsorbed mercury will be released from the surface of sorbents at 80 °C and totally evaporated at 360 °C according to the aforementioned TPD analysis. Therefore, 320 °C was chosen as the thermal regeneration temperature. As shown in Fig. 12, five cycles of mercury adsorption and regeneration were carried out in the reusability test. It can be seen that the mercury removal efficiency was kept almost the same as the first cycle of adsorption. The excellent regeneration performance of silver based sorbents was also proved by the study of Xu [11] and Dong [13]. The results indicated that Fe_3O_4/Ag composites could be promising low-cost mercury sorbents due to the ability of efficiently regenerating and being reused.

3. DFT Calculations

3-1. Hg^0 Interaction with Fe_3O_4(111)

Previous studies that have used the DFT calculations to investigate Hg^0 interaction with γ-Fe_2O_3 [33] and α-Fe_2O_3 [34] proposed that Fe^{3+} showed stronger activity for the reaction of mercury than O^{2-}. It can be inferred that the interaction of mercury and Fe^{3+} was more favorable. Furthermore, the Fe_3O_4(111) surface terminated with Fetet1 was confirmed to possess several adsorption active sites [20], which might be active to adsorb mercury. Herein, the Fetet1 site and the neighbor O-top site on the Fe_3O_4(111) surface were taken into consideration in the current work as depicted in Fig. 13. The Hg atom was placed perpendicularly toward the Fetet1 atom and O-top atom at the distance of 3.107 Å and 3.078 Å, respectively, which is depicted in Fig. 13(a) and (b). After geometry optimization, the configuration optimization of Fetet1 site is depicted in Fig. 13(c) and shows no obvious geometry change, and the Hg-Fe bond length was shortened to 2.805 Å. For the configuration optimization of O-top site, however, dramatic changes are observed in Fig. 13(d). The Hg-O bond stretched (3.520 Å) and

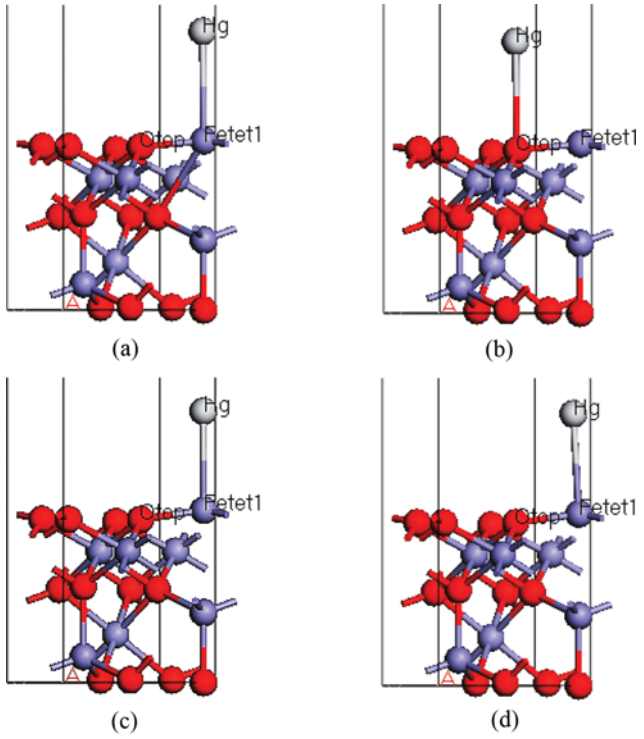

Fig. 13. Adsorption configurations of Hg^0 on the Fe_3O_4(111) surface ((a) and (b): The configuration of Fetet1 site and O-top site before adsorption, respectively; (c) and (d): The configuration of Fetet1 site and O-top site after adsorption, respectively).

Hg atom moved to Fetet1 site with the Hg-Fe bond length of 2.846 Å. It can be concluded that Hg^0 was more favorable to adsorbed on Fetet1 site stably, which is similar to the adsorption behavior of Hg^0 on γ-Fe_2O_3(001) [34] and α-Fe_2O_3(001) [34]. The calculated adsorption energy of Hg^0 on Fetet1 site and O-top site was −44.24 kJ/mol and −39.69 kJ/mol, respectively. Hence, the configuration of Hg^0 adsorbed on Fetet1 site is more stable. The adsorption energy of the this configuration is weaker than that of Hg^0 on γ-Fe_2O_3(001) perfect surface with the value of −54.3 kJ/mol [33], but stronger than that of Hg^0 on α-Fe_2O_3(001) [34] surface with the value of −37.66 kJ/mol. However, all of them belong to weak chemisorption.

3-2. Hg^0 Interaction with Ag/Fe_3O_4(111)

Geng et al. investigated the adsorption of Hg^0 on the Pd/γ-Al_2O_3(110) surface, in which Pd atom was primarily placed on the γ-Al_2O_3(110) surface, and then Hg atom started to adsorb [35]. From the characterization of the as-synthesized Fe_3O_4/Ag sorbent, silver existed on the surface of the Fe_3O_4 particles. So we carried out our work of Hg^0 interaction with Ag/Fe_3O_4(111) as follows: First, an Ag atom was placed perpendicular toward the center of the Fe_3O_4(111) surface, and then this configuration was optimized to obtain the final structure as shown in Fig. 14(a). Second, the Hg atom was placed perpendicular toward the Ag atom. After the geometry optimization the stable configuration was acquired and exhibited in Fig. 14(b). The calculated adsorption energy of this system was at the value of −86.82 kJ/mol, which was almost twice

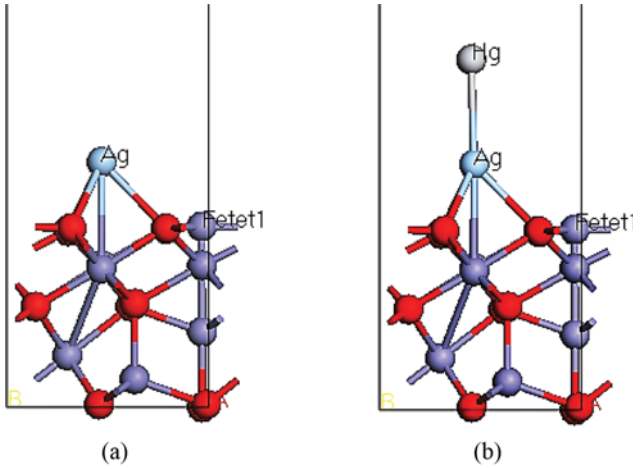

Fig. 14. Adsorption configurations of Hg^0 on the Ag/Fe_3O_4(111) surface ((a) The configuration before adsorption; (b) The configuration after adsorption).

as much of the bare Fe_3O_4(111) surface adsorption energy. It is confirmed that this interaction belongs to a strong chemisorption. Considering the above, we can conclude that the silver could greatly improve the Hg^0 removal performance of Fe_3O_4 sorbent, which agrees very well with our experiments results.

CONCLUSION

The magnetic Fe_3O_4/Ag nanocomposite was successfully synthesized and characterized by XRD, TEM, and EDS, which proved the existence of silver on the surface. A series of fixed-bed experiments were performed to test the mercury removal efficiency of the Fe_3O_4 and Fe_3O_4/Ag sorbents. The effects of the flue gas components, the adsorption temperature, the Hg^0 inlet concentration and the gas hourly space velocity on the Hg^0 removal efficiency were all evaluated on both sorbents. The results indicated that the loading of silver on the surface of Fe_3O_4 could significantly enhance the Hg^0 removal efficiency of the sorbents. Flue gas components, including CO_2, SO_2, and NO, have little impact on the mercury removal performance of Fe_3O_4/Ag sorbents, while O_2 has a slightly positive effect. For both sorbents, the Hg^0 removal efficiency of the both sorbents was decreased with the increasing of temperature, Hg^0 inlet concentration and gas hourly space velocity. Besides, the Hg^0 removal efficiency of Fe_3O_4/Ag sorbents was always higher than that of bare Fe_3O_4 sorbents under various conditions. The mercury species on solid surface was determined by TPD method and only one broad peak emerged at approximately 210 °C, which meant that mercury species existing on the surface of the sorbents might be elemental mercury instead of oxidized mercury. The reusability of the Fe_3O_4/Ag sorbents was also tested and a good ability of efficient regeneration and reuse was found, which indicated that the Fe_3O_4/Ag sorbents could be promising mercury removal sorbents.

The DFT calculations of the adsorption of mercury on the both sorbents were finally carried out in the current study. The DFT calculation of Hg^0 adsorbed on bare Fe_3O_4(111) surface and Ag/Fe_3O_4(111) surface indicated that the former belonged to weak chemisorption and the latter was strong chemisorption. The interaction of mercury with iron was more favorable than that of mercury with oxygen. The theoretical analysis agreed with our experiments very well and could provide an insightful understanding of the adsorption of mercury.

ACKNOWLEDGEMENTS

The authors gratefully acknowledge the support from the National Natural Science Foundation of China (No. 51476031, 51676040) and the development and application demonstration of high precision on-line monitoring technology for mercury speciation/concentration (No. 2016YFC0201105).

REFERENCES

1. E. Schuster, *Water Air Soil Poll.*, **56**, 667 (1991).
2. K. S. Park, Y. C. Seo, S. J. Lee and J. H. Lee, *Powder Technol.*, **180**, 151 (2008).
3. K. C. Galbreath and C. J. Zygarlicke, *Fuel Process. Technol.*, **65**, 289 (2000).
4. Y. Gao, Z. Zhang, J. Wu, L. Duan, A. Umar, L. Sun, Z. Guo and Q. Wang, *Environ. Sci. Technol.*, **47**, 10813 (2013).
5. S. Zhao, Z. Qu, N. Yan, Z. Li, W. Zhu, J. Pan, J. Xu and M. Li, *Rsc Adv.*, **5**, 30841 (2015).
6. B. Padak and J. Wilcox, *Carbon*, **47**, 2855 (2009).
7. S. J. Miller, G. E. Dunham, E. S. Olson and T. D. Brown, *Fuel Process. Technol.*, **65**, 343 (2000).
8. Y. Cao, H. Cui, W. P. Pan and J. Anal. *Appl. Pyrol.*, **80**, 319 (2007).
9. E. J. Granite, C. R. Myers, W. P. King, D. C. S. And and H. W. Pennline, *Ind. Eng. Chem. Res.*, **45**, 4844 (2006).
10. G. Luo, H. Yao, M. Xu, X. Cui, W. Chen, R. Gupta and Z. Xu, *Energy Fuels*, **24**, 419 (2009).
11. H. Xu, Z. Qu, W. Huang, J. Mei, W. Chen, S. Zhao and N. Yan, *Colloid Surf., A.*, **476**, 83 (2015).
12. D. Jie, Z. Xu and S. M. Kuznicki, *Adv. Funct. Mater.*, **19**, 1268 (2009).
13. J. Dong, Z. Xu and S. M. Kuznicki, *Environ. Sci. Technol.*, **43**, 3266 (2009).
14. C. Rungnim, J. Meeprasert, M. Kunaseth, A. Junkaew, P. Khamdahsag, P. Khemthong, N. Pimpha and S. Namuangruk, *Chem. Eng. J.*, **274**, 132 (2015).
15. Y. S. Kang, S. Risbud, J. F. Rabolt and P. Stroeve, *Chem. Mater.*, **8**, 2209 (1996).
16. X. Zhang, W. Jiang, X. Gong and Z. Zhang, J. *Alloys Compd.*, **508**, 400 (2010).
17. B. Delley, *J. Chem. Phys.*, **113**, 7756 (2000).
18. J. P. Perdew, K. Burke and M. Ernzerhof, *Phys. Rev. Lett.*, **77**, 3865 (1996).
19. B. Delley, *Phys. Rev. B*, **66**, 155125 (2002).
20. T. Yang, X. D. Wen, Y. W. Li, J. Wang and H. Jiao, *Surf. Sci.*, **603**, 78 (2009).
21. T. Su, Z. Qin, G. Huang, H. Ji, Y. Jiang and J. Chen, *Appl. Surf. Sci.*, **378**, 270 (2016).
22. P. Dementyev, K. H. Dostert, F. Ivars-Barceló, C. P. O'Brien, F.

Mirabella, S. Schauermann, X. Li, J. Paier, J. Sauer and H. J. Freund, *Angew. Chem. Int. Ed.*, **54**, 13942 (2015).
23. T. Yang, X.-D. Wen, C.-F. Huo, Y.-W. Li, J. Wang and H. Jiao, *J. Mol. Catal. A: Chem.*, **302**, 129 (2009).
24. X. Li and J. Paier, *J. Phys. Chem. C*, **2**, 120 (2016).
25. R. Nowakowski, J. Pielaszek and R. Duś, *Appl. Surf. Sci.*, **199**, 40 (2002).
26. F. Kong, J. Qiu, H. Liu, R. Zhao and Z. Ai, *J. Environ. Sci.*, **23**, 699 (2011).
27. L. Zhao, C. Li, X. Zhang, G. Zeng, J. Zhang and Y. E. Xie, *Catal. Sci. Technol.*, **5**, 3459 (2015).
28. S. J. Long and D. R. Scott and R. J. Thompson, *Anal. Chem.*, **45**, 2227 (1973).
29. Y. Liu, J. Zhang and J. Pan, *Energy Fuels*, **28**, 2135 (2014).
30. S. Zhao, Z. Qu, N. Yan, Z. Li, W. Zhu, J. Pan, J. Xu and M. Li, *Rsc Adv.*, **5**, 30841 (2015).
31. W. Hou, J. Zhou, C. Yu, S. You, X. Gao and Z. Luo, *Ind. Eng. Chem. Res.*, **53**, 9909 (2014).
32. P. Wang, S. Hu, J. Xiang, S. Su, L. Sun, F. Cao, X. Xiao and A. Zhang, *P. Combust. Inst.*, **35**, 2847 (2015).
33. P. Guo, X. Guo and C. Zheng, *Appl. Surf. Sci.*, **256**, 6991 (2010).
34. P. Guo, X. Guo and C. Zheng, *Fuel*, **90**, 1840 (2011).
35. L. Geng, L. Han, W. Cen, J. Wang, L. Chang, D. Kong and G. Feng, *Appl. Surf. Sci.*, **321**, 30 (2014).